IEEE Access
Multidisciplinary ⋮ Rapid Review ⋮ Open Access Journal

Received 8 December 2022, accepted 16 December 2022, date of publication 20 December 2022,
date of current version 28 December 2022.

Digital Object Identifier 10.1109/ACCESS.2022.3231098

RESEARCH ARTICLE

Robot-Aided Contactless Monitoring of Workers' Cardiac Activity in Hazardous Environment

ROBERTO CITTADINI[1,2], LUCA ROSARIO BUONOCORE[1], ELOISE MATHESON[1], MARIO DI CASTRO[1], AND LOREDANA ZOLLO[2], (Senior Member, IEEE)

[1]European Organization for Nuclear Research, 1211 Meyrin, Switzerland
[2]CREO Laboratory—Advanced Robotics and Human-Centred Technologies, Campus Bio-Medico University of Rome, 00128 Rome, Italy

Corresponding author: Roberto Cittadini (roberto.cittadini@cern.ch)

This work was supported by the European Council for Nuclear Research (CERN) budget for knowledge transfer for the benefit of medical applications.

This work involved human subjects in its research. The authors confirm that all human subject research procedures and protocols are exempt from review board approval.

ABSTRACT Vital signals monitoring is expected to support people in their daily activities in the near future, following continuous strides in developing health technologies for complex and hazardous environments. As the industry 4.0 revolution grows, robotic systems are increasingly deployed to support health monitoring, even though current robotic systems merely enable navigation and exploration of the surrounding environment to find people to be monitored, without adaptation of their behaviour to improve the quality of the health monitoring. At the European Organization for Nuclear Research (CERN), a wireless personnel safety prototype has been developed to assist workers in harsh environments, although this system needs to be improved in terms of invasiveness and portability. This work proposes a novel contactless approach based on a robotic system that adapts its behaviour to improve the performance of imaging-based algorithm for continuous physiological monitoring. Specifically, cardiac activity is monitored from camera views to obtain non-invasive and reliable vital parameter measurements. An extensive experiment has been conducted with ten healthy volunteers. The participants' heart rates were monitored at different distances and different camera zoom levels from the robotic system, and synchronously measured by a heart rate benchmark device for the ground truth. The results highlighted several distance-zoom combinations that can be reached by the robotic system to adapt its behaviour to the boundary conditions in order to minimize the heart rate measurement error during algorithm calculations. These distance-zoom combinations are used to implement the control of the robotic system, improve the heart rate calculation algorithm and overcome the limitations of previous systems. A comparison with previous works in the literature involving the cardiac activity algorithm reveals a consistent contribution of the robot-assisted contactless monitoring system in reducing the mean absolute error in heart rate estimation.

INDEX TERMS Human-centred robotic, robot vision system, safety, health monitoring.

I. INTRODUCTION

Vital parameters monitoring is necessary to assess a person's health state, track their physical or mental exertion and prevent dangerous situations appearing or escalating. Hazardous environments can pose risks for human health, due to the presence of dangerous elements and the high complexity of the unstructured working space [1].

At the European Organization for Nuclear Research (CERN) accelerator complex and experiments [2], the Large Hadron Collider (LHC) is the largest machine in the world, built in a tunnel of 27 km length 100 meters underground with only 8 access points from the surface [3]. Besides the long distances to be covered inside the tunnel and an unstructured environments characterized by machines and objects with

The associate editor coordinating the review of this manuscript and approving it for publication was Yizhang Jiang.

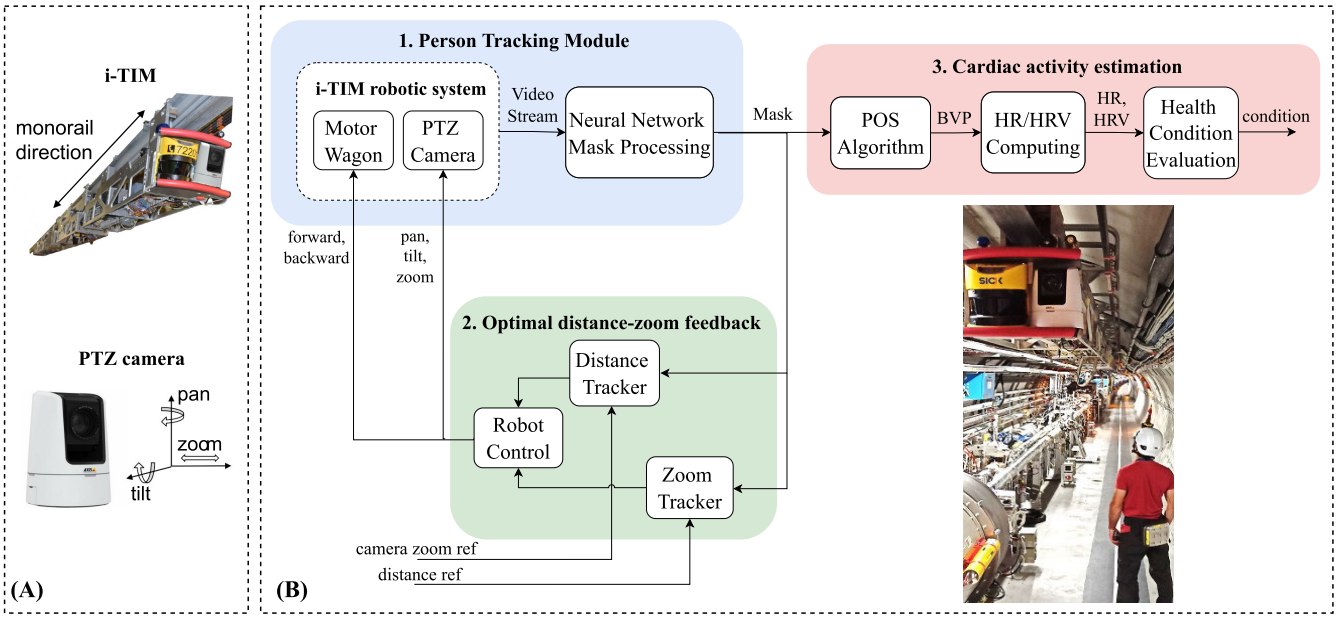

FIGURE 1. (A) Forward and backward movements of the i-TIM along the monorail and Pan-tilt-zoom camera; (B) Control workflow of robot-aided contactless monitoring of CERN worker's cardiac activity using the i-TIM robotic system: 1) Person Tracking Module (blue); 2) Optimal Distance-Zoom Feedback (green); 3) Cardiac Activity Estimation (red).

different possible configurations or states, human hazards present in CERN accelerators are mainly caused by radiation, oxygen deficiency, high temperature, loss of cognition of work time and high magnetic fields [4]. There is the need to identify workers' localization and to monitor their vital parameters, especially when they need to perform complex activities such as installations and maintenance works of heavy machinery.

A wireless personnel safety system prototype (WPSS) [5] was developed with the intention of measuring environmental parameters and also the heart rate of workers. This was initially tested by maintenance workers of the ATLAS detector [6]. The main comments from the participants highlighted the need to reduce the prototype size, minimize its invasiveness for long-term operations and improve its power consumption for portability.

Contact-based health monitoring in harsh environments has been widely explored with wearable devices, skin-applied electrodes, smartwatches, or smart belts at chest level [7], [8]. Contactless monitoring has proven to be a robust, hygienic, safe, and cost-effective alternative suitable for continuous long-distance and long-term monitoring [9], [10], [11]. As the Industry 4.0 revolution grows [12], robotic systems are also making significant strides in aiding and monitoring people at risk. In literature, most recent studies have presented human health monitoring systems to measure vital parameters in several harsh environments, such as:

(i) construction and industrial field, monitoring mining workers at high altitudes in extreme climatic conditions [13], heat stress monitoring in firefighting [14] and search for surviving workers through the detection of vital signs in emergency situations [15];

(ii) highly contagious scenarios due to the COVID-19 pandemic where agile mobile robotic platforms equipped with sensors are teleoperated by a trained operator to monitor the patient at risk and avoid direct contact by medical personnel [16], [17], [18];

(iii) unstructured environments, i.e. the home of an elderly person [19], [20], [21].

Although the above mentioned studies involve the presence of a robot [15], [16], [17], [18], [19], [20], [21], the robotic system has not been used to enhance the quality of the health monitoring: the robotic systems are merely deployed to enable the navigation and exploration of the surrounding environment to find people to be monitored, without adjusting their setting and adapting their position to the human in order to improve the accuracy of the health monitoring algorithm. Though wearable sensors can be a valid option for the general public, they are unsuitable for monitoring CERN workers. Besides the aforementioned issues raised by ATLAS maintenance workers themselves regarding first prototype [6], wearable sensors are limited to measuring short- term work sessions, due to any sensor displacement from the correct body positioning, the discomfort of long-duration work activities and the acceptability of the worker in wearing them [22], [23]. Moreover, any wearable device should be personal, one for each worker, or should be equipped with disposable electrodes thus increasing the cost and decreasing the viability and eco-sustainability of the system [24].

The objective of this work is to propose a novel contactless approach for robot-aided health monitoring of cardiac activity, where the robotic system plays an active role, adapts its configuration, and adjusts its placement, leading both to

improved performance of the image-based estimation algorithm and to reliable values of cardiac parameters.

The robot-aided contactless monitoring system is composed of:

(i) a robotic system capable of covering and exploring the entire LHC tunnel length, well described in detail in the section II-A;
(ii) a tracking module to search and follow workers;
(iii) an estimation module to measure workers' cardiac activity in a contactless way;
(iv) closed-loop control based on optimal distance-zoom configurations to allow the robotic system to act in achieving lower heart rate error values compared with previous works in the literature and in obtaining reliable performance from the cardiac activity estimation module.

The validation of the proposed system has been carried out by conducting an extensive experiment with ten healthy volunteers in the LHC tunnel mock-up, an environment present at CERN specially designed to faithfully reproduce the characteristics of the particle accelerator's tunnel. The participants' heart rate values have been recorded in contactless way via camera and compared with the benchmark device ones, evaluating the error between the values measured by the two different systems and their correlation by statistical analysis. Furthermore, a comparison has been carried out with previous works that involve cardiac activity algorithm to compare the system with the state-of-the-art in terms of mean absolute error.

II. MATERIALS AND METHODS

A. THE PROPOSED ROBOT-AIDED CONTACTLESS MONITORING SYSTEM

The robot-aided contactless monitoring system is shown in Figure 1A and consists of the following hardware components:

- Intelligent Train Inspection Monorail (i-TIM) [25]: developed at CERN, i-TIM is a robotic system that covers the LHC length of 27 km running on a monorail on the ceiling. This translational motion may be performed at a maximum speed of 10 km/h. The i-TIM robotic system is designed to support human work in radioactive areas. It is composed of multiple wagons, each with a length of 180 cm and with a precise task: control wagon, battery wagon, motor wagon, payload wagon and reconnaissance wagon. Due to its modular mechanical design and control architecture, the configuration can be adapted to different needs and scenarios. It has a 4G modem for communication with the CERN network on the surface, enabling remote operations and data transmission. The communication with i-TIM may also be established through Wi-Fi when close to the tunnel access points.
- Pan-Tilt-Zoom camera (PTZ camera) by AXIS Communications: this is a steerable mobile camera lens that is an integral part of the i-TIM. One is mounted on each end of the robotic train to perform visual inspections of the surroundings and to search for human presence. The main features are: 1920×1080 Full HD 1080p maximum resolution; x30 optical zoom and x12 digital one; Pan amplitude $\pm$ 170°and tilt range $-20°$ to 90°; horizontal field of view 62.8-2.3°, vertical one 37.0-1.3°; communication via IP address.
- Graphics Processing Unit by NVIDIA GeForce GTX 1080: for processing video resolution of up to 30 frames per second rate (FPS).

The software components are the following:

- Neural Network (NN): semantic segmentation and pixel-based classification is realized to classify each pixel of an image as belonging to a particular class (face pixel or not). Semantic segmentation algorithms U-net, originally designed and first used for biomedical image segmentation [26], has been employed and adapted to the purpose of this work with the use of the deep learning library Pytorch [27] with CUDA [28]. The Deep Neural Network is composed of 4 layers. Data manipulation libraries used and initialisation values are listed in Table 1. The proposed model has been trained by using 80% of the randomly shuffled dataset and has been tested on the remaining 20% using CelebA dataset [29], that contains 202599 face images, each annotated with 40 binary labels indicating facial attributes such as hair colour, gender and age. The performance metric used to determine the accuracy of the model is Intersection over Union (IoU), which is the ratio of the area of overlap between prediction and ground-truth to the area of union. The model achieved an accuracy of 0.92. The contours of the human face are well identified and the mask process is successfully realized, regardless of colour skin tone, size and rotation of the face within the camera's field of view and even though the face view is from the side. The model is adopted for dynamic mask processing of the human face and skin pixel detection from background ones.
- Plane-Orthogonal-to-Skin Algorithm (POS): remote photoplethysmography method (PPG) to extract pulsatile information from face skin pixels. Light is absorbed in a different way by blood contained in blood vessels compared to surrounding tissues [30]. This manifests itself on the surface of the skin with slight colour variations. Specular reflection is a mirror-like light reflection from the skin surface that is also affected by body motion, and does not contain any pulsatile information. Diffuse reflection is the light which penetrates the skin, and it is reflected and scattered inside skin tissues. Its value varies according to changes in blood volume, and it contains pulsatile information [31]. The POS algorithm is implemented due to its high performance and robustness in terms of skin-tone diversity, luminance, and recovery after a low, medium, or high effort [32]. Temperature may lead to variations in facial

TABLE 1. Software specifications, initialisation values, libraries and dependencies.

Software set-up	
Libraries	*Python v3.10.6* *Scipy (v1.9.1), Numpy (v1.23.3), Pandas (v1.5.0), Torch (v1.11.0), OpenCV (v3.4.1)*
Neural Network	*CelebA database, batchsize: 32, epochs: 50, learning rate: 1e-5*

skin colour on a large time scale (in the order of minutes). This slow colour variation due to temperature does not affect the estimation of the heart rate, which occurs every second. The algorithm suppresses the baseline colour (specular reflection) and considers only the colour changes of the skin due to the heart rate. Due to this operating principle, the algorithm is able to estimate the heart rate independently of the person's complexion, which is the tonic component and is filtered out. Physiological parameters that can be detected are Heart Rate (HR) and Heart Rate Variability (HRV), which provide important information about vital conditions [33].

The three main modules of the proposed novel architecture for robot-aided contactless monitoring system are shown in Figure 1B, including the (i) People Tracking Module, (ii) Optimal Distance-Zoom Feedback and (iii) Cardiac Activity Estimation.

1) PEOPLE TRACKING MODULE

The i-TIM can explore the surrounding environment with both the steerable PTZ camera and the translational motion of the entire robotic system along the monorail, thanks to the power provided by the motor wagon. A visual inspection begins with a continuous video recording of the LHC environment until a human presence enters the field of view (FOV) of i-TIM and a person is recognized by the system as a target to be monitored. Based on the camera-to-human distance, measured on the target axis, the i-TIM begins to approach the human target by physically moving along the ceiling monorail and adjusting the camera zoom to properly identify the human face.

The PTZ camera is coupled with a tracking algorithm that allows the robotic system to track and follow the movement of the person within the FOV [34]. This module positions and keeps the human face in the central area of the field of view, setting the pan and tilt speeds of the camera to adapt any change in the position of the person's face to the view of the camera itself [35]. If the human target is in opposition to the robotic train and therefore their face is hidden, i-TIM may exploit both the translational motion along the monorail to physically overtake the person and the switch from the PTZ camera of the first wagon to the one of the last wagon and vice versa.

The video stream is processed by the Neural Network (NN), which receives the video frames at 30 FPS and

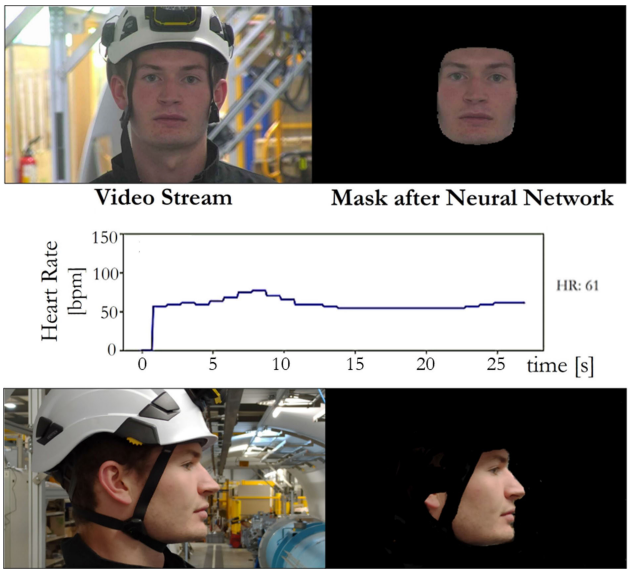

FIGURE 2. The Neural Network is applied to video stream and can detect the front and side of the human face for mask processing. Skin pixels are employed for the extraction of the blood volume pulse and heart rate time series.

constantly performs the segmentation of the human face mask: background pixels are discarded while skin pixels are considered for the next steps, as shown in Figure 2. The NN can also successfully detect the human face even with the side view, although the system has to manage the loss of about half of the face skin pixels to provide an adequate number of skin pixels input for the cardiac activity algorithm. The output of the module is a face mask containing the skin pixels, that is the input both for the "Cardiac Activity Estimation" module for monitoring vital parameters and the "Optimal Distance-Zoom Feedback" module for closed-loop control to adjust the current face mask.

2) OPTIMAL DISTANCE-ZOOM FEEDBACK

This module aims to find the optimal configuration of the i-TIM combining the PTZ camera lens movements in terms of pan, tilt and zoom with the linear translational motion of the robotic train along the monorail in order to provide the best input conditions for the imaging-based algorithm, described in section II-A3. A configuration consists of a distance-zoom combination, in terms of PTZ camera zoom and camera-human distance, to which a certain human face mask is associated. An optimal configuration implies a correct distance-zoom setup that allows to create a proper human face mask in terms of size, pose and number of skin pixels, in order to minimize measurement error and obtain reliable cardiac parameters.

To achieve this, a "Distance Tracker" block compares the current camera zoom with the camera zoom reference, relative to the current camera-human distance, measured on the lens axis. The "Zoom Tracker" block compares the current camera-human distance with the reference one, relative to the current camera zoom. The "Robot Control" block sends

commands to the i-TIM motor wagon for the translational motion and to the PTZ camera for the pan, tilt and zoom movements according to the information provided by the previous blocks.

3) CARDIAC ACTIVITY ESTIMATION

The POS algorithm projects a temporally normalized RGB signal, which is represented by the proportion of red, green and blue in the colour measured by skin pixel in a video, in the projection direction where the PPG high quality signal lies. This procedure minimizes any noise to obtain reliable pulse information.

The POS algorithm includes spatial averaging over each RGB channel, temporal normalization, projection, tuning and overlap-adding stages. The spatial averaging is represented by the following vector:

$$C(t) = [R(t), G(t), B(t)]^{\mathrm{T}}$$

where $R(t)$, $G(t)$ and $B(t)$ are the averaging pixel values of red, green and blue at time-instant t, respectively. The interval time of 5 s data of $C(t)$ is collected, and temporal normalization C_n performed. The channel-wise normalized vector is projected to two signals [19], [32] as:

$$S_n = \begin{bmatrix} S_1 \\ S_2 \end{bmatrix} = \begin{bmatrix} 0 & 1 & -1 \\ -2 & 1 & 1 \end{bmatrix} C_n$$

The projection indicates that the first signal S_1 is combined with the positive green channel and negative blue channel, and the second signal S_2 is combined with the negative double of red channel, positive green and blue channels. Then, the projected two signals are tuned as;

$$h_n = S_1 + \frac{\sigma(S_1)}{\sigma(S_2)} S_2$$

where $\sigma(*)$ is a standard deviation. The value h_{n} is collected for 5 s, which provides the 5 s window of the PPG signal. Processing time to estimate the heart rate value is 290 ms for a 5-second window. The procedure is repeated with a 1 s overlap so that the Heart Rate (HR) estimation results are obtained and displayed every 1 s by the "HR/HRV Computing" block in beats per minute (bpm), as shown in Figure 2. Moreover, two time domain metrics of the Heart Rate Variability (HRV) are extracted [36]: the standard deviation of the time interval between two successive normal heart beats (sDNN) and the root mean square of successive heart beats (rMSSD). The spectral characteristics of the signal for heart rate calculation tend to cover a frequency range from 0.75 Hz (45 bpm) to 3 Hz (180 bpm) [37]. The "Health Condition Evaluation" block provides the final output, i.e. the worker's condition, which may be safe or not depending on whether the heart parameters are above or below the standard physiological range [38]. Figure 3 illustrates the stages for cardiac activity estimation using the POS algorithm.

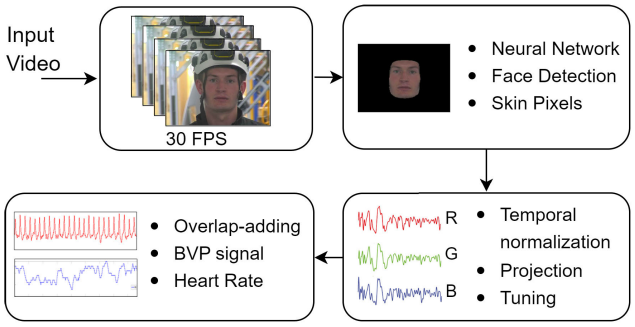

FIGURE 3. Block diagram of the stages of cardiac activity estimation using the POS algorithm.

B. EXPERIMENTAL SETUP AND PROTOCOL

Ten subjects were involved in the experiments (8 males, 2 females, 25.7 ± 2.8 years old). The number of participants in the experiment has been selected with reference to previous published studies concerning photoplethysmography [39], [40], [41]. The volunteers are welcomed into the LHC mock-up, where environmental conditions similar to the real case are reproduced, as shown in Figure 4, and introduced to the experiment. Each participant has been adequately informed about the purpose of the study and provided written informed consent before starting the experimental session. Moreover, each participant was asked to wear safety equipment commonly provided for CERN workers (i.e. helmet, safety shoes and work garment). The subjects were asked to stand assuming a posture that was natural and comfortable for them, while i-TIM robotic system was moving at different distance levels, in particular at camera-human distances of 1 m, 2.5 m, 5 m, 8 m and 10 m. For each distance, the PTZ camera zoom was scanned from the minimum value of x1 to the maximum of x30 for a time interval of 90 s for each zoom level. The subjects were not required to look at the i-TIM robotic system, as it was not strictly necessary for the estimation of their cardiac activity. The proposed robot-aided contactless monitoring system found the participant's face placed in its FOV and measured the instantaneous HR values. In addition to the heart rate values measured by the POS algorithm, the subjects wore a benchmark device at wrist level during the entire session of data collection. The cardiac activity was measured synchronously by a Shimmer3 ECG benchmark device to supply the ground truth for comparison. Furthermore, some preliminary experiments were conducted to evaluate the performance of the system in less favourable operating conditions. The heart rate was measured from the human face during: i) motion and talking; ii) participant lateral orientation (side-face).

C. EVALUATION METRICS

The evaluation metrics used to assess the performance of the proposed robot-aided contactless monitoring system consist of the following indicators:

- *Absolute Error* (AE): it compares the POS algorithm results with the Shimmer3 ECG results. As indicated

FIGURE 4. Experimental setup in the LHC mock-up: participant stands within the FOV of the robotic system and wears helmet, safety garment and benchmark device at wrist level for the ground truth.

in [42], the absolute error is a performance accuracy indicator of the PPG methods and it is calculated as follows:

$$AE(i) = |HR_{POS}(i) - HR_{true}(i)|$$

where $HR_{POS}(i)$ is the heart rate estimation from POS algorithm in the i-th window and $HR_{true}(i)$ is the true value of heart rate in beats per minute (bpm) provided by the benchmark device.

- *Mean Absolute Error* (MAE): it represents the overall evaluation of the cardiac activity estimation in a time interval of HRs collection in bpm unit.

$$MAE = \sum_{i=1}^{N} AE(i)$$

MAEs are calculated both for the first data collection with a static fixed camera and for the data collected with the PTZ camera mounted on the i-TIM mobile robotic system.

- *Sample Standard Deviation* (SD): measures the amount of variation or dispersion of the set of values.

$$SD = \sqrt{\frac{\sum_i (HR_{POS}(i) - HR_{true}(i))^2}{N-1}}$$

Low SD indicates that the values tend to be close to the mean of the set. A high SD denotes that the values are distributed over a wider range.

- *Pearson Correlation Coefficient* (ϱ): is the ratio between the covariance of two variables and the product of their standard deviations. It is a measure of linear correlation between two sets of data, i.e. heart rate values detected by POS algorithm and by the benchmark device. Pearson Correlation Coefficient value is between -1 and 1, which indicates the relationship between the two variables: weak correlation ($0 < |\varrho| < 0.3$), moderate ($0.3 < |\varrho| < 0.7$), and strong correlation ($|\varrho| > 0.7$).

$$\varrho = \frac{\sum_i (HR_{POS}(i) - \mu)(HR_{true}(i) - \hat{\mu})}{\sqrt{\sum_i (HR_{POS}(i) - \mu)^2} \sqrt{\sum_i (HR_{true}(i) - \hat{\mu})^2}}$$

where μ and $\hat{\mu}$ are respectively mean value of heart rate from POS algorithm and from Shimmer3 ECG benchmark device. In particular, the coefficient is used to assess the level of correlation between the two set of data at the optimal distance-zoom configurations, in which the mean heart rate error is lower.
The p-value is calculated alongside the Pearson Correlation Coefficient to assess the statistical significance of the correlation between the two set of data detected by the algorithm and by the benchmark device, referring to the statistics methodology of Nunan et al. [43] and Hsiao et al. [44]. If the p-value is less than the set threshold (p-value < 0.01), the correlation is statistically significant.

- *Mask ratio*: it provides an indication of face mask size in terms of the number of skin pixels over the number of total resolution pixels. This value indicates the percentage of face skin pixels that are framed in the camera field of view. It is calculated as follows:

$$mask\ ratio \equiv \frac{skin\ pixel\ number}{total\ resolution\ pixels}\ [\%]$$

where total resolution pixel for PTZ camera was set at 921600 pixels (1280×720) HD.

III. RESULTS AND DISCUSSION

Figure 4 shows part of the data from the experimental sessions of three different participants: the heart rate value over time measured by the POS algorithm and the benchmark device are compared, and the relative graph of the Absolute Error with the Mean Absolute Error is shown.

Figure 5A shows that the HR_{POS} follows the trend of the HR_{true}, with a MAE lower than 2 bpm. The graph of the AE shows significant fluctuations, also reaching very high error peaks, such as 7.9 bpm at time 45 s and 9.6 bpm at time 63 s. In Figure 5B, the AE reaches the value of 18 bpm at time 38 s, however, the MAE of the session is 2.3 bpm. In Figure 5C, the AE reaches the value of 5 bpm in the interval 23-25 s and 6.3 bpm at the time 87 s.

The POS algorithm follows the increasing or decreasing trend of the heart rate with a slight delay compared with the heart rate measured by the reference device since the algorithm needs a short response time interval to change the HR_{POS} value to follow the real HR_{true} one measured by the benchmark device. Due to this, results show that the highest AE peaks are found at the steepest slope changes

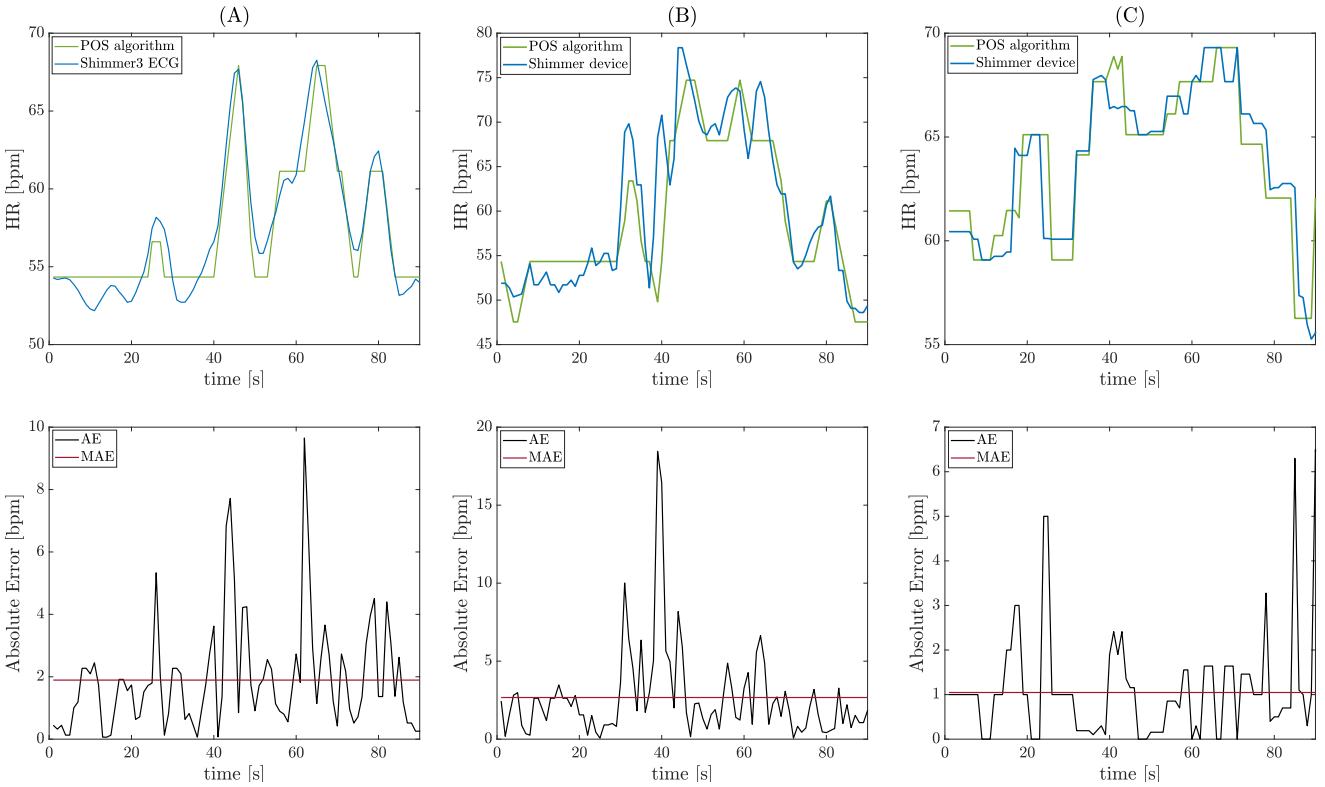

FIGURE 5. (A)-(B)-(C): comparison between heart rate measurements performed using the POS algorithm and the Shimmer3 ECG benchmark device for a representative subject during 90 s experimental session; Absolute Error between the two measurements. The red line represent the mean value.

TABLE 2. Numerical values of the Mean Absolute Error (MAE) averaged over all the 10 participants. The highlighted MAEs have an error value below 2 bpm and identify the optimal configurations of distance-zoom combination.

MAE	4x	6x	8x	10x	12x	14x	16x	18x	25x	30x
1 m	**0.8 ± 0.3**	**1.3 ± 0.9**	**1.9 ± 1.2**	3.0 ± 1.6	6.1 ± 2.0	7.2 ± 2.8	8.1 ± 1.8	8.2 ± 2.1	8.8 ± 0.9	9.0 ± 2.6
2.5 m	3.1 ± 1.2	**1.7 ± 1.3**	**0.8 ± 0.4**	**0.9 ± 0.3**	**1.3 ± 1.0**	2.5 ± 1.1	2.3 ± 0.8	6.2 ± 2.7	5.3 ± 2.5	6.5 ± 2.2
5 m	5.6 ± 1.5	5.0 ± 2.8	2.8 ± 1.3	2.1 ± 1.8	**1.0 ± 0.8**	**0.9 ± 0.5**	**1.6 ± 1.0**	3.7 ± 1.2	3.0 ± 1.0	6.7 ± 2.9
8 m	8.3 ± 1.5	7.4 ± 2.1	7.3 ± 2.3	5.4 ± 1.5	3.2 ± 1.3	**1.1 ± 1.0**	**1.2 ± 0.7**	**1.9 ± 1.5**	4.3 ± 1.3	5.5 ± 2.1
10 m	8.9 ± 2.0	9.1 ± 2.8	8.8 ± 3.5	8.3 ± 2.9	7.5 ± 2.5	7.1 ± 3.2	7.5 ± 1.5	4.7 ± 2.1	3.5 ± 1.2	**1.0 ± 0.6**

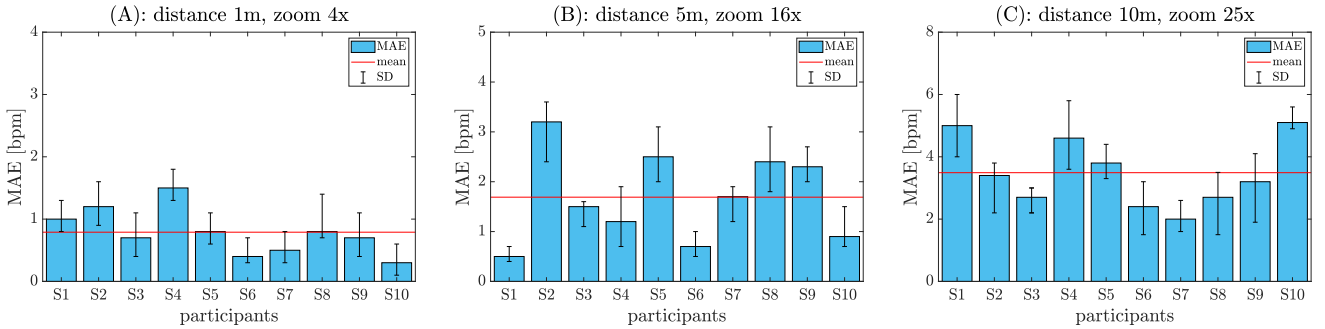

FIGURE 6. Mean Absolute Error and Standard Deviation for each participants at (a) distance 1 m, zoom 4x (b) distance 5 m, zoom 16x and (c) distance 10 m, zoom 25x. MAE average is shown over all participants (red line).

in heart rate and last for a short interval of time (between 1-3 s) that correspond to the time of responsiveness of the POS algorithm in adapting to the real heart rate. The different responsiveness is explained by the different modes of heart

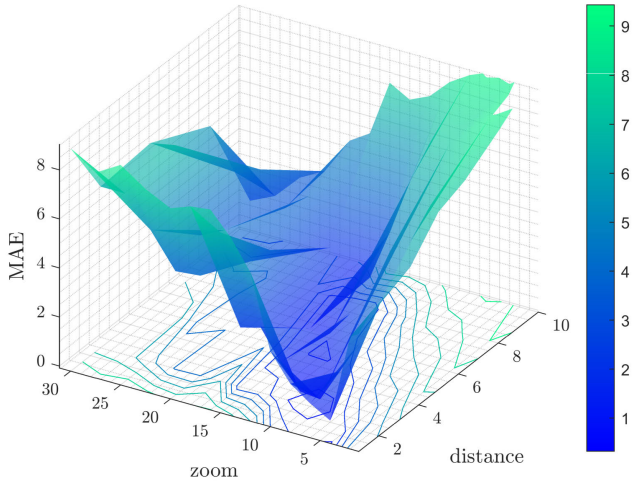

FIGURE 7. Mean Absolute Error (MAE) in relation to zoom and distance. Distance-zoom couple identifies an i-TIM robotic configuration. Each configuration has a different MAE value. There are configurations more suitable than others for heart rate estimation.

rate sensing, i.e. contact-based and contactless, and by the different spatial distances that blood has to flow forward the different areas, i.e. wrist and face, after being pumped from the heart [45].

The results of the experiment reveal that some video conditions may provide a more appropriate input mask for the POS algorithm than others, which positively affect its performance and minimizes the error in heart rate estimation. Specifically, several distance-zoom combinations are identified as more suitable than others for measuring human cardiac activity using imaging photoplethysmography via the camera stream.

Table 2 reports MAE values averaged over all ten participants. Several distance-zoom combinations represent an optimal configurations for heart rate measurement with i-TIM robotic system. As highlighted in the Table 2, the lowest MAE recorded is 0.8 bpm, achieved at distance-zoom combination of 1m-4x and of 2.5m-8x. Moreover, configurations with a MAE$\leq$1 bpm and 1 bpm $<$ MAE $<$ 2 bpm are also highlighted in Table2, which provide reliable estimation of cardiac activity.

In Figure 6, the MAEs of each participant with Standard Deviation (SD) and the mean over all participants (red line) are shown in histograms for three different distance-zoom combinations:

- In Figure 6A, MAEs of each participant at distance of 1 m with a camera zoom of 4x. The highest MAE of 1.5 bpm is recorded for subject S4 and the lowest one of 0.4 bpm for S10. The mean MAE over all participants for this distance-zoom combination is 0.8 bpm;
- In Figure 6B, MAEs of each participant at distance of 5 m with a camera zoom of 16x are shown. The highest MAE of 3.2 bpm is recorded for S2 and the lowest one of 0.5 bpm for S1. The mean MAE over all participants for this distance-zoom combination is 1.6 bpm;

TABLE 3. Performance comparison in terms of Mean Absolute Error (MAE) of the HR estimation using POS algorithm reported in recent studies.

Work	Year	Dataset	MAE (bpm)
A. Unakafov et al. [46]	2018	DEAP	1.99
A. Gudi et al. [47]	2020	UBFC-rPPG	4.73
	2020	MMSE-HR	5.77
	2020	VIPL-HR	11.5
E. Lee et al. [48]	2020	UBFC-rPPG	4.12
R. Song et al. [49]	2021	UBFC-rPPG	4.05
L. Lampier et al. [50]	2022	22 subjects	1.77
POS + Robot-aided	-	10 subjects	**1.25**

- In Figure 6C, MAEs of each participant at distance of 10 m with a camera zoom of 25x are shown. The highest MAE of 5.1 bpm is recorded for S10 and the lowest one of 2 bpm for S7. The mean MAE over all participants for this distance-zoom combination is 3.5 bpm.

As regards spectral characteristics of the signal, frequencies are between 0.87 Hz and 1.35 Hz, as 52 bpm for participant S4 and 81 bpm for participant S9 are the minimum and maximum heart rates recorded during the experiment, respectively.

In Figure 7, the Mean Absolute Error (MAE) value averaged over all participants is shown graphically in relation to the PTZ camera zoom and to the camera-human distance: zoom range is up to 30x, distance range from 1 to 10 m. Furthermore, the most recent studies evaluating the performance of the POS algorithm using Mean Absolute Error (MAE) are considered. Table 3 reports the MAE values observed in other studies compared to the value obtained in the present work. The MAE value of 1.25 bpm is the average of the MAEs obtained for the optimal distance-zoom configurations identified above. The value obtained shows how the contribution of the robotic system in achieving the optimal configurations leads both to a consistent improvement in the performance of the POS algorithm and to a reliable measurement of the heart rate with a lower error.

Table 4 shows Pearson Correlation Coefficient and the relative p-value calculated for the optimal distance-zoom combinations. Results denote a strong correlation between the heart rate by the POS algorithm and the ground truth by the benchmark device, as Pearson's correlation coefficient is higher than $\varrho > 0.7$ for all optimal distance-zoom configurations: minimum is $\varrho = 0.87$ for 5 m distance and 14x zoom and maximum is $\varrho = 0.96$ for 8 m distance and 16x zoom. In general, for most distance-zoom combinations, the ϱ coefficient is higher than 0.9. Furthermore, the associated p-value indicates that the correlation found with ϱ coefficient is statistically significant, since p-value is largely below than 0.01 for all the distance-zoom combinations.

The algorithm performance evaluated on participants with lateral orientation reveals that the heart rate is not negatively affected if the person's face is lateral. In contrast, for motion and talking activity, the mean absolute error is increased by +3.7 bpm, thus leading to an MAE of 4.95 bpm. However,

TABLE 4. Correlation of heart rate value measured with POS algorithm and Shimmer3 ECG benchmark device for optimal configurations of distance-zoom: Pearson Correlation Coefficient (PCC) values show strong correlation and p-value denotes that it is statistically significant.

distance-zoom	PCC	p-value
d = 1m, zoom = 4x	ρ = 0.92	p < 0.0001
d = 1m, zoom = 6x	ρ = 0.92	p = 0.0009
d = 1m, zoom = 8x	ρ = 0.92	p = 0.0012
d = 2.5m, zoom = 6x	ρ = 0.92	p = 0.0004
d = 2.5m, zoom = 8x	ρ = 0.94	p = 0.0007
d = 2.5m, zoom = 10x	ρ = 0.89	p < 0.0001
d = 2.5m, zoom = 12x	ρ = 0.94	p < 0.0001
d = 5m, zoom = 12x	ρ = 0.90	p = 0.0014
d = 5m, zoom = 14x	ρ = 0.87	p < 0.0001
d = 5m, zoom = 16x	ρ = 0.91	p = 0.0005
d = 8m, zoom = 14x	ρ = 0.91	p < 0.0001
d = 8m, zoom = 16x	ρ = 0.96	p = 0.0002
d = 8m, zoom = 18x	ρ = 0.92	p = 0.0008
d = 10m, zoom = 30x	ρ = 0.92	p = 0.0004

this value is still comparable and even better than other values presented in the literature and reported in Table 3.

Data analysis over all the participants highlights that the key factor in obtaining a low-value error in heart rate estimation is related to mask processing: it is crucial to provide a proper input mask to the POS algorithm, which consists of an adequate number of skin pixels to achieve minimal heart rate error. Figure 8 compares the MAE with the mask ratio, whose value is directly proportional to the number of skin pixels in the mask. The optimal results in terms of low error are obtained when the mask ratio is between 26.0% and 35.5% for a MAE less than 2 bpm. For values above or below this mask ratio range, MAE increases towards higher values. A general pattern is found: for a mask ratio > 35.5%, the $HR_{POS}(i)$ is underestimated compared to the real value $HR_{true}(i)$, meanwhile for mask ratio < 26.0%, an overestimation occurs compared to the real one. This is critical during the monitoring of a person from the side-face, as a large number of skin pixels cannot be used to measure cardiac activity since they are covered from the opposite side. The lost skin pixels must be compensated by a larger mask size, within the range of 26.0% < mask ratio < 35.5%, which allows a thicker number of the video pixels and thus more skin pixels to perform correct heart rate measurements using the POS algorithm.

To this regard, robotic systems that support human activity are paramount for tasks that require extreme precision and repetitive movements, such as finding and keeping these specific distance-zoom configurations. The contribution of the robotic system is important to increase the reliability and precision of heart rate monitoring and to achieve accurate and continuously updated adjustment based on the person's

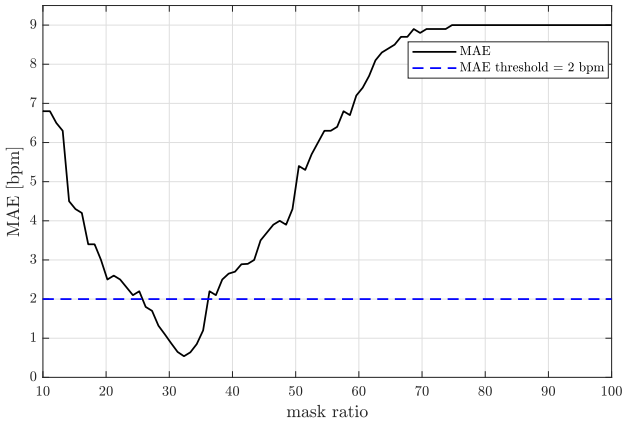

FIGURE 8. MAE values vary with mask ratio, which represent the percentage of skin pixel number in the resolution window of 1280 × 720.

position in the LHC tunnel: the appropriate distance-zoom configurations can be accurately reached and maintained by robot-aided contactless monitoring, which adjust its behaviour in terms of translational motion and the PTZ camera zoom, in order to measure a reliable cardiac activity estimation with minimal heart rate error. Starting from its current configuration, i-TIM moves along the monorail and sets the PTZ camera zoom to reach close configuration with a low MAE. The system does not affect the daily workers' routine: the robot-aided contactless monitoring system adapts its behaviour to the human being and not vice versa, thus providing a human-centred health monitoring exploiting a robotic system.

From the experimental results, the distance-zoom coordinates, relative to the lower MAE values, are considered. In a specific LHC tunnel spot, skin pixels number contained in the mask are conditioned by PTZ camera zoom and the person-robot distance. It is well known that moving the i-TIM train along the monorail rather than zooming the PTZ camera is a completely different task from an energy expenditure point of view: the former is certainly more expensive, therefore it affects battery life and robot availability. A necessary assessment must be made regarding the robotic system energy saving. However, studies are underway to make the i-TIM robotic system constantly recharge to have unlimited battery life.

In Figure 9, the robotic system has the zoom set to 2x and identifies a person 5 m away from its lens (current configuration). The mean average error is around 7 bpm with this distance-zoom settings. Since it is a high error, i-TIM must switch to a new configuration that provides a lower MAE in order to have a more reliable cardiac activity estimation. The closest two configurations with a MAE<1 bpm are shown in Figure 9. The robotic system selects to follow the path towards the configuration with MAE value of 1.0, despite the error numerical value is higher than its neighbour MAE of 0.8. The first path involves only a change in camera zoom from 2x to 14x, while second path involves a movement of 2.5 m along the monorail, as well as a change in zoom

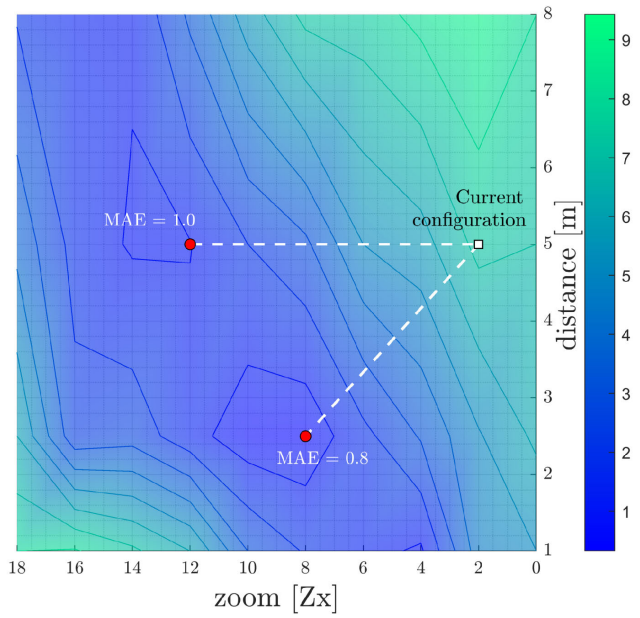

FIGURE 9. The current configuration is set to camera-human distance of 5m and 2x zoom. The robotic system moves to other configurations with a lower MAE, considering energy savings.

from 2x to 8x. A higher accuracy in calculating heart rate is not worthwhile as it involves more battery consumption. When the error is considered negligible,the i-TIM is satisfied with an estimation that is still excellent, but achieved with a lower expenditure of energy in order to have the robot system available for other tasks and for more time.

IV. CONCLUSION

This work has proposed a novel approach to a robot-aided health contactless monitoring in which the robotic system has an active role in improving the imaging-based algorithm performance in cardiac activity estimation. The system also provides a solution that satisfies the requirements of CERN workers as a valid alternative to the previous developed prototype. The proposed approach has been tested on ten subjects in the LHC tunnel mock-up environment.

The results obtained from the data analysis revealed that there are some distance-zoom combinations that allow the i-TIM robotic system to reach an optimal configuration and measure heart rate value with an average error of less than 2 bpm (sometimes even less than 1 bpm). The robotic system does not only navigate the surrounding environment to search for people, it also actively participates in increasing the performance of the POS algorithm and in achieving the best configuration for a proper mask, in terms of size and skin pixels number, a reliable heart rate estimation, and battery saving. The comparison with the most recent studies using the POS algorithm in the literature has been conducted: the MAE value of 1.25 bpm obtained in this work reveals how the contribution of the robotic system as an active system in reaching the optimal configurations and adjusting its position leads to a consistent improvement in the performance of the POS algorithm respect with to the previous works, and to a heart rate measurement with a lower error. Furthermore, the contactless strategy ensures non-invasive and continuous monitoring of people during daily work activities to meet their expectations, as workers stated during the interview.

The limitations of the system are related to illumination and fast facial movements, which affect the system output by introducing relevant fluctuations in heart rate values. Since the scenario and its ambient light are known in advance (i.e. LHC tunnel), currently the model parameters are fine-tuned first according to the environmental scenario in which the system will be operated.

Future work will focus on the following areas:

1) widen the set of physiological parameters detectable through PPG-based methods and extend the range of measurements to multiple individuals simultaneously;
2) evaluate the implementation of PTZ camera data and algorithm in the service of healthcare personnel in medical scenarios;
3) Validation of the system in the real operational setting: deepen the limits of the system to make it more responsive to people's movements, make it automatically adapted to changes in ambient light over time, and mitigate possible drops in the accuracy of heart rate measurements.

ACKNOWLEDGMENT

Personal and Sensitive Data were processed in the scope of scientific research in the context of CERN's specific activities (legal basis par. 28.5 and 29.5 of OC 11).

REFERENCES

[1] M. Di Castro, M. Ferre, and A. Masi, "CERNTAURO: A modular architecture for robotic inspection and telemanipulation in harsh and semi-structured environments," *IEEE Access*, vol. 6, pp. 37506–37522, 2018.
[2] L. Evans, "Particle accelerators at CERN: From the early days to the LHC and beyond," *Technological Forecasting Social Change*, vol. 112, pp. 4–12, Nov. 2016.
[3] Y. Baconnier, G. Brianti, P. Lebrun, A. G. Mathewson, and R. Perin, "LHC: The Large Hadron Collider accelerator project," CERN, Geneva, Switzerland, 1993. [Online]. Available: https://cds.cern.ch/record/257706
[4] T. Otto, "Risks and hazards of particle accelerator technologies," in *Safety for Particle Accelerators*. Cham, Switzerland: Springer, 2021, pp. 5–54.
[5] M. F. Alam, E. Adamidi, and S. Hadjiefthymiades, "Wireless personnel safety system (WPSS), a baseline towards advance system architecture," in *Proc. 18th Panhellenic Conf. Informat. (PCI)*, 2014, pp. 1–6.
[6] A. Collaboration, G. Aad, E. Abat, J. Abdallah, A. A. Abdelalim, A. Abdesselam, O. Abdinov, B. A. Abi, M. Abolins, and H. Abramowicz, "The atlas experiment at the Cern large hadron collider," *J. Instrum.*, vol. 3, Aug. 2008, Art. no. S08003.
[7] I. Awolusi, E. Marks, and M. Hallowell, "Wearable technology for personalized construction safety monitoring and trending: Review of applicable devices," *Autom. Construction*, vol. 85, pp. 96–106, Jan. 2018.
[8] A. Lanata, A. Greco, S. Di Modica, F. Niccolini, F. Vivaldi, F. Di Francesco, C. Tamantini, F. Cordella, L. Zollo, M. Di Rienzo, C. Massaroni, E. Schena, M. Di Sarto, and E. P. Scilingo, "A new smart-fabric based body area sensor network for work risk assessment," in *Proc. IEEE Int. Workshop Metrology for Ind. 4.0 (IoT)*, Jun. 2020, pp. 187–190.
[9] D. Nhan Tran, H. Lee, and C. Kim, "A robust real time system for remote heart rate measurement via camera," in *Proc. IEEE Int. Conf. Multimedia Expo (ICME)*, Jun. 2015, pp. 1–6.
[10] Y. Cho, S. J. Julier, N. Marquardt, and N. Bianchi-Berthouze, "Robust tracking of respiratory rate in high-dynamic range scenes using mobile thermal imaging," *Biomed. Opt. Exp.*, vol. 8, no. 10, pp. 4480–4503, 2017.

[11] R. Sinhal, K. Singh, and M. Raghuwanshi, "An overview of remote photoplethysmography methods for vital sign monitoring," in *Computer Vision and Machine Intelligence in Medical Image Analysis*. Cham, Switzerland: Springer, 2020, pp. 21–31.

[12] M. A. K. Bahrin, M. F. Othman, N. H. N. Azli, and M. F. Talib, "Industry 4.0: A review on industrial automation and robotic," *J. Teknologi*, vol. 78, nos. 6–13, Jun. 2016.

[13] P. Aqueveque, C. Gutiérrez, F. S. Rodríguez, E. J. Pino, A. S. Morales, and E. P. Wiechmann, "Monitoring physiological variables of mining workers at high altitude," *IEEE Trans. Ind. Appl.*, vol. 53, no. 3, pp. 2628–2634, May/Jun. 2017.

[14] G. Florea, R. Dobrescu, D. Popescu, and M. Dobrescu, "Wearable system for heat stress monitoring in firefighting applications," in *Proc. 2nd Int. Conf. Inf. Technol. Comput. Netw. (ITCN13)*, 2013, pp. 129–134.

[15] A. Ivanovs, A. Nikitenko, M. Di Castro, T. Torims, A. Masi, and M. Ferre, "Multisensor low-cost system for real time human detection and remote respiration monitoring," in *Proc. 3rd IEEE Int. Conf. Robotic Comput. (IRC)*, Feb. 2019, pp. 254–257.

[16] H.-W. Huang et al., "Agile mobile robotic platform for contactless vital signs monitoring," *TechRxiv*, 2020, doi: 10.36227/techrxiv.12811982.v1.

[17] G.-Z. Yang, B. J. Nelson, R. R. Murphy, H. Choset, H. Christensen, S. H. Collins, P. Dario, K. Goldberg, K. Ikuta, N. Jacobstein, D. Kragic, R. H. Taylor, and M. McNutt, "Combating COVID-19—The role of robotics in managing public health and infectious diseases," *Sci. Robot.*, vol. 5, no. 40, Mar. 2020, Art. no. eabb5589.

[18] C. Tamantini, F. Scotto di Luzio, F. Cordella, G. Pascarella, F. E. Agro, and L. Zollo, "A robotic health-care assistant for COVID-19 emergency: A proposed solution for logistics and disinfection in a hospital environment," *IEEE Robot. Autom. Mag.*, vol. 28, no. 1, pp. 71–81, Mar. 2021.

[19] H. Lee, H. Ko, H. Chung, and J. Lee, "Robot assisted instantaneous heart rate estimator using camera based remote photoplethysmograpy via plane-orthogonal-to-skin and finite state machine," in *Proc. 42nd Annu. Int. Conf. IEEE Eng. Med. Biol. Soc. (EMBC)*, Jul. 2020, pp. 4425–4428.

[20] P. Zhao, C. X. Lu, B. Wang, C. Chen, L. Xie, M. Wang, N. Trigoni, and A. Markham, "Heart rate sensing with a robot mounted mmWave radar," in *Proc. IEEE Int. Conf. Robot. Autom. (ICRA)*, May 2020, pp. 2812–2818.

[21] S. Cosar, Z. Yan, F. Zhao, T. Lambrou, S. Yue, and N. Bellotto, "Thermal camera based physiological monitoring with an assistive robot," in *Proc. 40th Annu. Int. Conf. IEEE Eng. Med. Biol. Soc. (EMBC)*, Jul. 2018, pp. 5010–5013.

[22] J. L. Martin, E. Murphy, J. A. Crowe, and B. J. Norris, "Capturing user requirements in medical device development: The role of ergonomics," *Physiological Meas.*, vol. 27, no. 8, pp. R49–R62, Aug. 2006.

[23] A. Spagnolli, E. Guardigli, V. Orso, A. Varotto, and L. Gamberini, "Measuring user acceptance of wearable symbiotic devices: Validation study across application scenarios," in *Proc. Int. Workshop Symbiotic Interact.* Cham, Switzerland: Springer, 2015, pp. 87–98.

[24] C. Dincer, R. Bruch, E. Costa-Rama, M. T. Fernández-Abedul, A. Merkoçi, A. Manz, G. A. Urban, and F. Güder, "Disposable sensors in diagnostics, food, and environmental monitoring," *Adv. Mater.*, vol. 31, May 2019, Art. no. 1806739.

[25] M. Di Castro, M. L. B. Tambutti, M. Ferre, R. Losito, G. Lunghi, and A. Masi, "I-TIM: A robotic system for safety, measurements, inspection and maintenance in harsh environments," in *Proc. IEEE Int. Symp. Saf., Secur., Rescue Robot. (SSRR)*, Aug. 2018, pp. 1–6.

[26] O. Ronneberger, P. Fischer, and T. Brox, "U-Net: Convolutional networks for biomedical image segmentation," in *Proc. Int. Conf. Med. Image Comput. Computer-Assisted Intervent.* Cham, Switzerland: Springer, 2015, pp. 234–241.

[27] P. Mishra, "Introduction to neural networks using PyTorch," in *PyTorch Recipes*. Cham, Switzerland: Springer, 2019, pp. 111–126.

[28] H. Jang, A. Park, and K. Jung, "Neural network implementation using CUDA and OpenMP," in *Proc. Digit. Image Computing, Techn. Appl.*, 2008, pp. 155–161.

[29] Z. Liu, P. Luo, X. Wang, and X. Tang, "Large-scale celebfaces attributes (celeba) dataset," *Retrieved August*, vol. 15, no. 2018, p. 11, 2018.

[30] H. W. Loh, S. Xu, O. Faust, C. P. Ooi, P. D. Barua, S. Chakraborty, R.-S. Tan, F. Molinari, and U. R. Acharya, "Application of photoplethysmography signals for healthcare systems: An in-depth review," *Comput. Methods Programs Biomed.*, vol. 216, Apr. 2022, Art. no. 106677.

[31] R. M. Fouad, O. A. Omer, and M. H. Aly, "Optimizing remote photoplethysmography using adaptive skin segmentation for real-time heart rate monitoring," *IEEE Access*, vol. 7, pp. 76513–76528, 2019.

[32] W. Wang, A. C. den Brinker, S. Stuijk, and G. de Haan, "Algorithmic principles of remote PPG," *IEEE Trans. Biomed. Eng.*, vol. 64, no. 7, pp. 1479–1491, Jul. 2017.

[33] G. E. Billman, H. V. Huikuri, J. Sacha, and K. Trimmel, "An introduction to heart rate variability: Methodological considerations and clinical applications," *Front. Physiol.*, vol. 6, p. 55, Feb. 2015.

[34] H. K. Chavda and M. Dhamecha, "Moving object tracking using PTZ camera in video surveillance system," in *Proc. Int. Conf. Energy, Commun., Data Analytics Soft Comput. (ICECDS)*, Aug. 2017, pp. 263–266.

[35] Y. Cai and G. Medioni, "Persistent people tracking and face capture using a PTZ camera," *Mach. Vis. Appl.*, vol. 27, no. 1, pp. 397–413, Apr. 2016.

[36] F. Shaffer and J. P. Ginsberg, "An overview of heart rate variability metrics and norms," *Frontiers Public Health*, vol. 5, p. 258, Sep. 2017.

[37] D. J. McDuff, E. B. Blackford, and J. R. Estepp, "Fusing partial camera signals for noncontact pulse rate variability measurement," *IEEE Trans. Biomed. Eng.*, vol. 65, no. 8, pp. 1725–1739, Aug. 2017.

[38] M. Malik, J. T. Bigger, A. J. Camm, R. E. Kleiger, A. Malliani, A. J. Moss, and P. J. Schwartz, "Heart rate variability: Standards of measurement, physiological interpretation, and clinical use," *Eur. Heart J.*, vol. 17, no. 3, pp. 354–381, 1996.

[39] F. Bousefsaf, C. Maaoui, and A. Pruski, "Automatic selection of webcam photoplethysmographic pixels based on lightness criteria," *J. Med. Biol. Eng.*, vol. 37, no. 3, pp. 374–385, 2017.

[40] M. B. Mashhadi, M. Essalat, M. Ahmadi, and F. Marvasti, "An improved algorithm for heart rate tracking during physical exercise using simultaneous wrist-type photoplethysmographic (PPG) and acceleration signals," in *Proc. 23rd Iranian Conf. Biomed. Eng. 1st Int. Iranian Conf. Biomed. Eng. (ICBME)*, 2016, pp. 146–149.

[41] H. E. Tasli, A. Gudi, and M. den Uyl, "Remote PPG based vital sign measurement using adaptive facial regions," in *Proc. IEEE Int. Conf. Image Process. (ICIP)*, Oct. 2014, pp. 1410–1414.

[42] Ž. Pirnar, M. Finžgar, and P. Podržaj, "Performance evaluation of rPPG approaches with and without the region-of-interest localization step," *Appl. Sci.*, vol. 11, no. 8, p. 3467, Apr. 2021.

[43] D. Nunan, G. Donovan, D. Jakovljevic, L. Hodges, G. Sandercock, and D. Brodie, "Validity and reliability of short-term heart-rate variability from the polar S810," *Medicine Sci. Sports Exercise*, vol. 41, no. 1, p. 243, 2009.

[44] C.-C. Hsiao, F.-W. Hsu, R.-G. Lee, and R. Lin, "Correlation analysis of heart rate variability between PPG and ECG for wearable devices in different postures," in *Proc. IEEE Int. Conf. Syst., Man, Cybern. (SMC)*, Oct. 2017, pp. 2957–2962.

[45] J. Fine, K. L. Branan, A. J. Rodriguez, T. Boonya-ananta, Ajmal, J. C. Ramella-Roman, M. J. McShane, and G. L. Coté, "Sources of inaccuracy in photoplethysmography for continuous cardiovascular monitoring," *Biosensors*, vol. 11, no. 4, p. 126, Apr. 2021.

[46] A. M. Unakafov, "Pulse rate estimation using imaging photoplethysmography: Generic framework and comparison of methods on a publicly available dataset," *Biomed. Phys. Eng. Exp.*, vol. 4, no. 4, Apr. 2018, Art. no. 045001.

[47] A. Gudi, M. Bittner, and J. van Gemert, "Real-time webcam heart-rate and variability estimation with clean ground truth for evaluation," *Appl. Sci.*, vol. 10, no. 23, p. 8630, Dec. 2020.

[48] E. Lee, E. Chen, and C.-Y. Lee, "Meta-rPPG: Remote heart rate estimation using a transductive meta-learner," in *Proc. Eur. Conf. Comput. Vis.* Cham, Switzerland: Springer, 2020, pp. 392–409.

[49] R. Song, H. Chen, J. Cheng, C. Li, Y. Liu, and X. Chen, "PulseGAN: Learning to generate realistic pulse waveforms in remote photoplethysmography," *IEEE J. Biomed. Health Informat.*, vol. 25, no. 5, pp. 1373–1384, May 2021.

[50] L. C. Lampier, C. T. Valadão, L. A. Silva, D. Delisle-Rodríguez, E. M. D. O. Caldeira, and T. F. Bastos-Filho, "A deep learning approach to estimate pulse rate by remote photoplethysmography," *Physiological Meas.*, vol. 43, no. 7, Jul. 2022, Art. no. 075012.

ROBERTO CITTADINI received the B.Sc. degree in medical engineering from the University of Rome "Tor Vergata," in 2017, and the M.Sc.Eng. degree in biomedical engineering and robotics from the Campus Bio-Medico University of Rome (Italy), in 2020. He is currently pursuing the Ph.D. degree with CERN, affiliated with the University Campus Bio-Medico of Rome in Advanced Robotics and Human–Centered Technologies Research Unit. In 2020, he joined CERN's Mechatronics, Robotics, and Operations Section as a Cooperation Associate (COAS) Engineer, working on health contactless monitoring of physiological parameters, using cameras, radars, and distance sensors. His research interests include worker monitoring in harsh environment, physiological signal analysis, and human–centered technologies.

LUCA ROSARIO BUONOCORE received the M.Sc. degree in electronic engineering from the University of Naples Federico II, Naples, Italy, and the Ph.D. degree in computer and automation engineering from the University of Naples Federico II, in 2015. He started as a Research Fellow at the European Organization for Nuclear Research (CERN), Geneva, Switzerland, where he is currently a Research Staff with the Research and Development Robotic Division of Mechatronics, Robotics, and Operations Section. His main research interests include mechatronic design of novel robotic solutions, such as mobile robotic platforms and ultralight robotic arms for a real manipulation for harsh environment application.

ELOISE MATHESON received the B.Sc. and B.Eng. degrees in mechatronics (space) engineering from The University of Sydney, Australia, in 2010, the M.Sc. degree in advanced robotics from École Central de Nantes, France, in 2014, and the Ph.D. degree in surgical robotics from the Imperial College London, U.K., in 2021. The subject of the Ph.D. was the research, development, and clinical evaluation of the human–machine interface of a novel steerable soft catheter for neurosurgery. From 2014 to 2016, she was an Engineer at the Telerobotics and Haptics Laboratory, European Space Agency, The Netherlands, largely working on telerobotic activities under the METERON project. In 2020, she joined CERN's Mechatronics, Robotics and Operations Section as a Mechatronics Engineer, working on beam intercepting device mechatronic systems and the development and integration of robotic solutions in the accelerator complex. Her research interests include tele-operation, supervisory control, autonomous operations, haptics, and human–machine interfaces.

MARIO DI CASTRO received the M.Sc. degree in electronic engineering from the University of Naples "Federico II", Italy, and the Ph.D. degree in robotics and industrial controls from the Polytechnic University of Madrid, Spain. From 2005 to 2006, he was an Intern and a Technical Student at CERN, where he was a in charge of advanced magnetic measurements and studies for LHC superconducting magnets. From 2007 to 2011, he works at EMBL c/o DESY in charge of advanced mechatronics solutions for synchrotron beamlines controls. Since 2011, he has been working at CERN, where he leads the Mechatronics, Robotics and Operation Section. The section is responsible for the design, installation, operation, and maintenance of advanced control systems based on different control platforms for movable devices characterized by few um positioning accuracy (e.g. scrapers, collimators, goniometers, and target) in harsh environment. Important section activities are the design, construction, installation, operation, and maintenance of robotic systems used for remote maintenance in the whole CERN accelerator complex and quality assurance. His research interests include modular robots, tele-robotics, human robot interfaces, machine learning, enhanced reality, automatic controls, mechatronics, precise motion control in harsh environment, and advanced robotics also for search and rescue scenarios.

LOREDANA ZOLLO (Senior Member, IEEE) received the M.S. degree in electronic engineering from Università degli Studi di Napoli "Federico II," in 2000, and the Ph.D. degree in bioengineering from Scuola Superiore Sant'Anna di Pisa, in 2004. She is a Full Professor of bioengineering and the Director of the Master of Science in Biomedical at Università Campus Bio-Medico di Roma (UCBM), where she is also the Director of the CREO Lab–Laboratory of Advanced Robotics and Human–Centered Technologies. She has been involved in more than 40 EU-funded and national projects in her application fields, such as the EU H2020/FET-Open/SOMA as a Project Coordinator and the EU H2020/ODIN and AIDE as a Scientific Coordinator for UCBM. She has authored/coauthored more than 160 scientific publications and six patents. Her research interests include rehabilitation and assistive robotics, biorobotics and bionics, human–machine interfaces, and collaborative robotics.